Influence of temperature and dry density coupled effects on HTO, ^{36}Cl, ^{85}Sr and ^{133}Ba diffusion through compacted bentonite

Miguel García-Gutiérrez , Manuel Mingarro , Tiziana Missana [*]

CIEMAT, Physical Chemistry of Actinides and Fission Products Unit Department of Nuclear Fission, Av. Complutense 40, 28040, Madrid, Spain

A B S T R A C T

This study investigated the combined impact of temperature (from 25 to 80 °C) and dry density of bentonite (from 1.2 to 1.65 g·cm^{-3}) on the apparent diffusion coefficient, D_a, of four radionuclides (HTO, ^{36}Cl, ^{85}Sr and ^{133}Ba) in a Ca-Mg bentonite. In this study, the different porewater chemistry, present under the specific experimental conditions – a factor often overlooked in diffusion studies – was explicitly considered. As a support to diffusion studies, batch sorption tests were carried out at different temperatures (25, 40, 60, and 80 °C) with the sorbing elements (^{85}Sr and ^{133}Ba).

The planar source method was used for the determination of apparent diffusion coefficients, D_a, which demonstrated its efficacy for both conservative (HTO and Cl) and sorbing elements. For all the investigated radionuclides, D_a values decreased with increasing the clay dry density and increased with increasing temperature. Notably, the highest D_a value ($1·10^{-9}$ m^2 s^{-1}) was attained for HTO diffusion in the clay at 1.2 g cm^{-3} and 80 °C, while the lowest D_a ($3.6·10^{-12}$ m^2 s^{-1}) value was determined for Ba diffusion at 1.65 g cm^{-3} and 25 °C.

The experimental D_a values were analysed employing the Arrhenius law and the Stokes-Einstein equations. Results revealed that diffusion data are in a reasonable agreement with Arrhenius behaviour, but deviations from the Stokes-Einstein equation were observed for compaction densities higher than 1.4 g cm^{-3}.

1. Introduction

Bentonite clay is extensively used for isolating hazardous materials, spanning from landfills to deep geological repositories for high-level radioactive waste (HLRW). Various methodologies for designing HLRW disposals, incorporating the utilization of compacted bentonite, have been documented across different countries (JNC, 1999; Enresa, 1999; Andra, 2001; Nagra, 2002; NEA, 2003; SKB, 2011; Posiva, 2012).

The disposal of HLRW relies on a multi-barrier system where the spent fuel is housed within metallic canisters encased by compacted bentonite. These engineered barriers are situated within a natural barrier, typically comprising crystalline or sedimentary rocks, which acts as the host formation for the waste storage (Savoye et al., 2011; Sellin and Leupin, 2014). Following repository closure, natural water from the host rock will hydrate and saturate the compacted bentonite, prompting it to swell and seal the voids volume. The decay of radioactive waste results in a temperature gradient extending from the canisters to the bentonite, with temperatures reaching up to 90–100 °C at the interface between the bentonite barrier and the canisters (Andra, 2005; Huertas et al., 2000).

Due to the low hydraulic conductivity and permeability of saturated bentonite, radionuclide diffusion through the bentonite is a crucial process in the context of HLRW disposal, being the predominant solute transport mechanism. Additionally, radionuclide sorption onto the bentonite influences their diffusion behaviour. Consequently, the study of radionuclide diffusion and sorption in bentonite under a range of relevant conditions, is indispensable for the safety assessment of HLRW disposals.

Radionuclide diffusion in bentonite depends on several factors: the physicochemical properties of the diffusing species; the characteristics of the solid (pore structure, degree of compaction, adsorption capability); the porewater chemistry, and temperature (Kozaki et al., 2001; Van Loon et al., 2004; García-Gutiérrez et al., 2006; Xiang et al., 2016; Medved and Černý, 2019), which often actuates simultaneously.

Several data on radionuclide diffusion as a function of clay dry density can be found in the literature (García-Gutiérrez et al., 2004, 2011; Idemitsu et al., 2016; Xiang et al., 2016; Pope, 2017; Joseph et al., 2017). Nevertheless, the effects of temperature have been scarcely analysed, and most of the available studies, varying temperature, were

performed with the non-sorbing (conservative) elements tritium (HTO) or deuterium (HDO) (González-Sánchez et al., 2008; Suzuki et al., 2004). Furthermore, the interpretation of results related to temperature effects is sometimes controversial: Rowe et al. (2005) studied HTO diffusion within a geosynthetic clay liner at 5 °C and 22 °C and found that mass transport was reduced at the lowest temperature. Savoye et al. (2011) studied HTO, ^{36}Cl, ^{22}Na and ^{137}Cs diffusion in the Callovo-Oxfordian claystone at 21 °C and 80 °C, and always obtained higher D_e values at 80 °C. Joseph et al. (2013) studied U(VI) diffusion in Opalinus clay, at 25 °C and 60 °C, and observed that D_e (effective diffusion coefficient) increased with temperature, but that clear variations on D_a could not be appreciated. Mon et al. (2016) studied Cl and K diffusion in compacted kaolinite and reported D_a values two times higher at 40 °C than at 6 °C; Bestel et al. (2018) performed through-diffusion experiment with HTO and ^{22}Na increasing the temperature from 0 °C to 80 °C in five steps, but could only determine, by the time-lag method, the diffusion coefficient at 25 °C. Zheng and Zaoui (2013) and Yang et al. (2015), studied water and cation diffusion as a function of temperature (between 240 K and 420 K), by means of molecular dynamics simulations. They concluded that the effect of temperature is negligible in weakly hydrated clay (1-layer hydrated), whereas it becomes significant in highly hydrated one (3-layer hydrated).

To our knowledge, no previous studies have investigated the combined effects of clay dry density and temperature on radionuclide diffusion, explicitly considering the chemical characteristics of pore water under varying experimental conditions, which are generally not accounted for in diffusion studies.

Thus, this study aims to determine the apparent diffusion coefficient (D_a) of four RNs (HTO, ^{36}Cl, ^{85}Sr, and ^{133}Ba) in bentonite, analysing the variation of the temperature (25, 40, 60, and 80 °C) and dry density (1.20, 1.40, and 1.65 g cm^{-3}). Tritiated water (HTO) is expected to be representative of all the chemical tracers that are not adsorbed by the solid phases (conservative); ^{36}Cl is also a conservative tracer but, being negatively charged, its diffusive transport can be affected by anion exclusion (García-Gutiérrez et al., 2004). Finally, ^{85}Sr and ^{133}Ba are sorbing tracers. Batch sorption tests were also carried out with these sorbing tracers at different temperatures and with different contact waters, as a support for diffusion studies.

The method selected for diffusion test is the instantaneous planar source method, which presents the advantage of avoiding the contact of tracers (especially the sorbing ones) with the experimental vessels, where sorption can also occur (Aldaba et al., 2010; García-Gutiérrez et al., 2011; Kasar et al., 2016).

The results of diffusion tests conducted at different dry densities and temperatures were evaluated using theoretical approaches as the Arrhenius law and the Stokes-Einstein equation; the results and discrepancies observed were discussed.

2. Materials and methods

2.1. Materials

2.1.1. Bentonite
The clay selected for these studies was the Spanish FEBEX bentonite, which has been studied in the frame of several international projects related to HLRW repositories (Enresa 1999; Huertas et al., 2000). The bentonite was extracted from the Cortijo de Archidona deposit (Almería, Spain); it is originated from volcanic materials altered by hydrothermal processes and has a high smectite content (93 ± 2 %), with quartz (2 ± 1 %), plagioclase (3 ± 1 %), cristobalite (2 ± 1 %), potassic feldspar, calcite, and tridymite as accessory minerals. The FEBEX bentonite is a Ca-Mg clay, with a cation exchange capacity (CEC) of (1.02 ± 0.04) 10^{-3} eq·g^{-1} and main exchanging cations Ca^{2+} (0.42 ± 0.03)·10^{-4} eq·g^{-1}; Mg^{2+} (0.32 ± 0.02)· 10^{-4} eq·g^{-1}; Na$^+$ (0.24 ± 0.02)·10^{-4} eq·g^{-1}; and K$^+$ (0.21 ± 0.02)·10^{-5} eq·g^{-1}. Its specific weight is 2.7 g

cm^{-3}. More detailed description of this material can be found in Huertas et al. (2000, 2006).

2.1.2. Contact waters
The porewater chemistry of the FEBEX bentonite at different dry densities was studied by Fernández and Rivas (2004). The composition of these waters is summarized in Table 1.

Synthetic porewaters (PW) were produced to saturate the bentonite, according to the selected dry density (PW (1.2); PW(1.4) and PW(1.65). The PW salinity increases with the dry density of the clay, according to a smaller pore volume where salts naturally present in the clay (e.g. halite and gypsum) can dissolve.

To analyse separately the possible effect of temperature on the water chemistry, additional tests were carried out placing the compacted clay at each density in ultrapure water at different temperatures (from 25 to 80 °C).

Table 2 shows the chemical composition of the water in contact with the samples compacted at 1.65 g/cm^3. Temperature also produces an increase of the salinity of the water in contact with the bentonite, in agreement with an increased solubility of the salts.

2.1.3. Tracers
HTO and ^{85}Sr were supplied by PerkinElmer Spain; ^{36}Cl by Isotope Products Laboratories, USA; and ^{133}Ba by Eckert & Ziegler Isotope Products, USA. HTO and ^{36}Cl are beta emitters and were measured, upon extraction from the solid, by liquid scintillation counting using a Tri-Carb 4910 TR PerkinElmer Liquid Scintillation Counter and Ultima Gold as scintillation cocktails. The cations ^{85}Sr and ^{133}Ba are γ emitters and their activity was measured using a Packard Auto-gamma Cobra II 5003, with a 3" NaI (Tl activated) crystal.

2.2. Batch sorption experiments

Batch sorption tests were carried out with ^{85}Sr and ^{133}Ba at different temperatures (25, 40, 60, and 80 °C) the solid to liquid ratio was 10 g L^{-1} and different contact waters were used: deionized water (DW) and the synthetic waters corresponding to clay porewater at 1.40 g cm^{-3} (PW 1.4) and 1.65 g cm^{-3} (PW 1.65).

The selected contact time for adsorption tests was one week. The solid and liquid phases were separated by centrifugation (21255 *g*, 30 min) with a JOUAN MR23i centrifuge. Three aliquots of the supernatant were extracted from each tube to measure the residual radionuclide activity in the liquid phase. The distribution coefficient, K_d (mL·g^{-1}) is calculated by the following expression:

$$K_d = \frac{C_0 - C_f}{C_f} \cdot \frac{V}{m} \qquad (1)$$

where C_0 and C_f represent the initial and final radionuclide concentration, *V* is the volume of the solution and *m* the mass of the solid.

Table 1
Chemical composition (mol·L^{-1}) of porewater as function of dry density.

Element	PW(1.2) 1.20 g cm^{-3}	PW(1.4) 1.40 g cm^{-3}	PW(1.65) 1.65 g cm^{-3}
Na$^+$	1.03·10^{-1}	1.13·10^{-1}	1.29·10^{-1}
K$^+$	9.43·10^{-4}	1.01·10^{-3}	1.11·10^{-3}
Mg^{2+}	1.35·10^{-2}	1.48·10^{-2}	1.71·10^{-2}
Ca^{2+}	1.27·10^{-2}	1.36·10^{-2}	1.54·10^{-2}
Cl$^-$	4.72·10^{-2}	6.36·10^{-2}	9.27·10^{-2}
SO$_4^{2-}$	5.04·10^{-2}	4.87·10^{-2}	4.52·10^{-2}
HCO$_3^-$	1.16·10^{-3}	1.10·10^{-3}	9.20·10^{-4}
pH	7.57	7.56	7.55
Cond. (mS/cm)	12.25	13.53	15.74
Ionic strength (M)	0.173	0.187	0.210

Table 2
Chemical composition (mol·L^{-1}) of ultrapure water in equilibrium with the bentonite at 1.65 g cm^{-3} and different temperature.

Element	25 °C	40 °C	60 °C	80 °C
Cl$^-$	1.58·10^{-4}	2.71·10^{-4}	5.64·10^{-4}	9.03·10^{-4}
HCO$_3^-$	4.92·10^{-5}	4.92·10^{-5}	4.69·10^{-5}	4.43·10^{-5}
SO$_4^{2-}$	1.56·10^{-5}	3.12·10^{-5}	8.12·10^{-5}	1.77·10^{-4}
Ca^{2+}	1.55·10^{-5}	1.70·10^{-5}	2.99·10^{-5}	3.24·10^{-5}
Mg^{2+}	4.94·10^{-6}	8.64·10^{-6}	1.56·10^{-5}	2.35·10^{-5}
Na$^+$	1.39·10^{-4}	3.31·10^{-4}	6.52·10^{-4}	9.13·10^{-4}
K$^+$	2.56·10^{-6}	4.60·10^{-6}	1.15·10^{-5}	1.76·10^{-5}
Si^{4+}	1.07·10^{-6}	3.92·10^{-6}	1.03·10^{-5}	2.10·10^{-5}
pH	6.85	7.12	7.46	7.63
Cond. (µS/cm)	66.2	137.4	179.2	228.0

Table 3
Theoretical porosity and moisture for 100 % saturation at each dry density. Theoretical moisture values can be compared with the experimental ones.

Dry density (g·cm^{-3})	Porosity (%)	Theoretical moisture (%)	Measured moisture (%)
ρ_d=1.20	55.55	46.30	47.3–48.4
ρ_d=1.40	48.15	34.39	35.4–36.8
ρ_d=1.65	38.89	23.57	20.3–22.2

2.3. Experimental set-up for diffusion tests

To perform diffusion tests, the bentonite was compacted at three different dry densities: 1.2, 1.4, and 1.65 g cm^{-3}. The clay was crushed and sieved (<1 mm, ASTM nº 18), its moisture was checked (~11 %) and then it was saturated with synthetic waters simulating the pore water composition of compacted bentonite at the three different densities. The synthetic water needed for reaching 100 % saturation was added previously to the compaction process. A hydraulic press was used to compact the weighted bentonite inside stainless-steel cylinders, with a diameter of 1.9 cm and a length of either 1 or 2 cm.

In the instantaneous planar source method, a thin radionuclide source is sandwiched between two compacted bentonite samples. In this configuration, symmetrical diffusion profiles are determined at the end of the experiment, after slicing the clay in thin sections (García-Gutiérrez et al., 2006). One end of the clay sample is closed with an end-piece of Delrin™, and two identical compacted parts of the diffusion cells are put together and separated by a filter paper (Whatman nº 54) impregnated with a tracer solution. After the placement of the filter paper, the two parts of the cell were assembled by means of another piece of Delrin™. A picture of the diffusion cell is shown in Fig. 1.

The filter paper contained 0.03 mL of tracer in all the experiments. The initial radionuclide concentration was 4.7·10^{-7} M, 4.35·10^{-4} M, 1.18·10^{-6} M, and 6.69·10^{-8} M, for HTO, ^{36}Cl, ^{85}Sr, and ^{133}Ba, respectively. These concentrations were selected because allowed an adequate detection of the radionuclide along the diffusion profile.

Diffusion tests were carried out at different temperatures (25, 40, 60, and 80 °C) and the cells were introduced into a *Controlled Environment* G25 chamber of New Brunswick Scientific in which temperature can be adjusted. After packing, the cell was wrapped in Parafilm™ to minimise water loss. The loss of water in bentonite produced by temperature increase, can modify its swelling capacity (Villar et al., 2010) and the total porosity of the sample, thus it must be avoided. After disassembling the cell, water saturation of the samples was verified weighting and drying all the slices obtained in the experiment.

Results are summarized in Table 3, which shows the theoretical porosity and moisture (water content) for each dry density for saturated samples, and the range of moisture measured after the tests completion, confirming that loss of water did not occur.

Bentonite samples of 1 or 2 cm length were used for HTO and ^{36}Cl experiments, which lasted between 2 and 6 h. The experiments with ^{85}Sr and ^{133}Ba were performed in 1 cm long clay samples, taking between 20 and 72 h to obtain measurable diffusion profiles. The range of duration of the experiments was initially determined by scoping calculations, according to the initial experimental conditions.

To measure the activity of beta emitters (HTO and ^{36}Cl) in the bentonite slices, it was necessary to extract the RN from the solid material first. Each slice was mixed with 8 mL of deionized water and stirred for three days before centrifugation. The resulting supernatant was then used to measure the radionuclide activity. The activity of gamma emitters (^{85}Sr and ^{133}Ba) was directly measured by placing the clay slices into polyethylene vials.

2.4. Mathematical description of planar diffusion source method

In the planar diffusion source method, the apparent diffusion coefficient, D_a, can be estimated analysing concentration profiles in the material. More details on the theoretical and experimental approximations for studying diffusion in compacted clays have been reported elsewhere (García-Gutiérrez et al., 2006).

D_a is related to the effective diffusion coefficient, D_e, distribution coefficient, K_d, porosity (ε) and bulk dry density (ρ_d) according to the following relation:

$$D_a = \frac{D_e}{\varepsilon + \rho_d \cdot K_d} \tag{2}$$

The radionuclide diffuses from the filter through both sides of the bentonite sample along the axial direction, resulting in a symmetrical concentration profile. To obtain the concentration profile within the solid, the radionuclide activity in each slice was measured, being the position and weight of each slice known. The tracer activity in the concentration profiles was fixed in the middle of the interval of each slice. The filter paper represents a sort of discontinuity in the system; thus, the simulations were carried out excluding this point.

The mathematical description of radionuclide diffusion in this configuration considers that a mass of tracer, M, is uniformly injected across the cross-section of area, A, of the clay at point $x = 0$ and time $t = 0$. The initial width of the tracer (thin source) is considered infinitesimally small and therefore the Dirac delta function, $\delta(x)$, can be used for the description of the tracer source at the initial conditions.

The initial and boundary conditions are:

C(x = 0, t = 0) = M/(δ(x)·A)

C(-∞ < x < ∞, t = 0) = 0

Fig. 1. Picture of the diffusion cell. Left: open cell; Right: assembled cell.

In this experimental configuration, D_a can be determined using the following analytical solution (Crank, 1975):

$$C(x,t) = \frac{M}{2A\sqrt{\pi D_a t}} \exp\left(-\frac{x^2}{4D_a t}\right) \qquad (3)$$

where $C(x,t)$ is the tracer concentration, M is the initial activity in the filter, A the cross-sectional area, x is the distance from the filter paper, and t is the experimental diffusion time.

The values of D_a were obtained by fit the experimental concentration profiles (C/M *vs*. x) using by least squares fit with Solver of Excel.

3. Results and discussion

3.1. Sorption tests

The results of the adsorption tests for Sr and Ba at different temperatures and contact waters (DW, PW(1.4), and PW(1.65)) are presented in Fig. 2.

Ba adsorption is observed to be always higher than that of Sr. The sorption of metal ions with the same charge is expected to depend on their ionic radius and hydration energies. Under the same experimental conditions, higher adsorption of Ba could be expected for its larger ionic radius ($Ba^{2+} = 1.34$ Å and $Sr^{2+} = 1.12$ Å), as experimentally observed.

The highest K_d values are observed in DW water, with a significant difference in adsorption between Ba and Sr, the former showing a higher affinity for the solid phase. In the PW (1.4) and PW(1.65), which have higher salinity, K_d values decreases by 2 orders of magnitude, but a large differences between the two porewaters is not observed. The strong dependence of adsorption on the ionic strength is expected for alkaline earth metals, which adsorb on clays mainly by cation exchange. Under the conditions of diffusion experiments, the K_d values for Ba (80-60 mL g^{-1}) and Sr (<10 mL g^{-1}) are not very high, and these tests underline the importance of considering realistic chemical conditions for comparing K_d values obtained in batch or diffusion tests.

Fig. 2 also shows that the increase in temperature results in a decrease in the distribution coefficient, particularly evident in the tests performed with DW (less ionic strength), but less strong under the more saline conditions given by PW 1.4 and PW 1.65, where salinity *per-se* significantly hinders the retention of these cations.
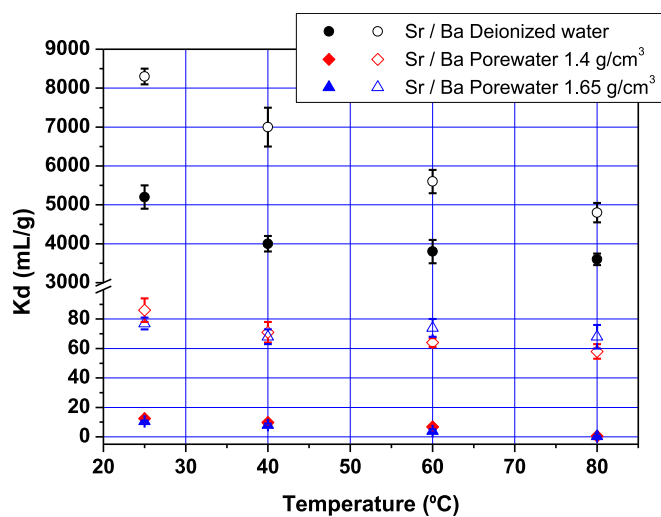
3.2. Diffusion experiments

Fig. 3 illustrates the diffusion profiles obtained using the planar source method and the simulation performed using Equation (3) to determine D_a under different experimental conditions. Fig. 3a displays the profiles obtained for HTO at different dry densities and a temperature of 80 °C, and Fig. 3b shows the profiles obtained for Ba under the same conditions. The symmetrical experimental profiles obtained on both sides of the clay sample were used to estimate the mean apparent diffusion coefficient for each test. The results for all the RN, dry densities, and temperatures, are summarized in Table 4.

A comparison of the diffusion behaviour of HTO and ^{133}Ba at the same dry density and temperature reveals that the distance travelled by ^{133}Ba is consistently lower than that of HTO. This suggests that the diffusion time needed for the sorbing element to develop concentration profiles as wide as those observed for the non-sorbing element is much higher (ranging from 2 to 72 h), in agreement with the expected retardation due to adsorption in the clay.

Despite being a non-sorbing species, the transport of ^{36}Cl differs from that of HTO in compacted clays due to the impact of electrostatic forces between the negatively charged clay surfaces and the anions. This leads to anionic exclusion, which reduces the volume of pore water available for anion transport and results in smaller values of D_a compared to those
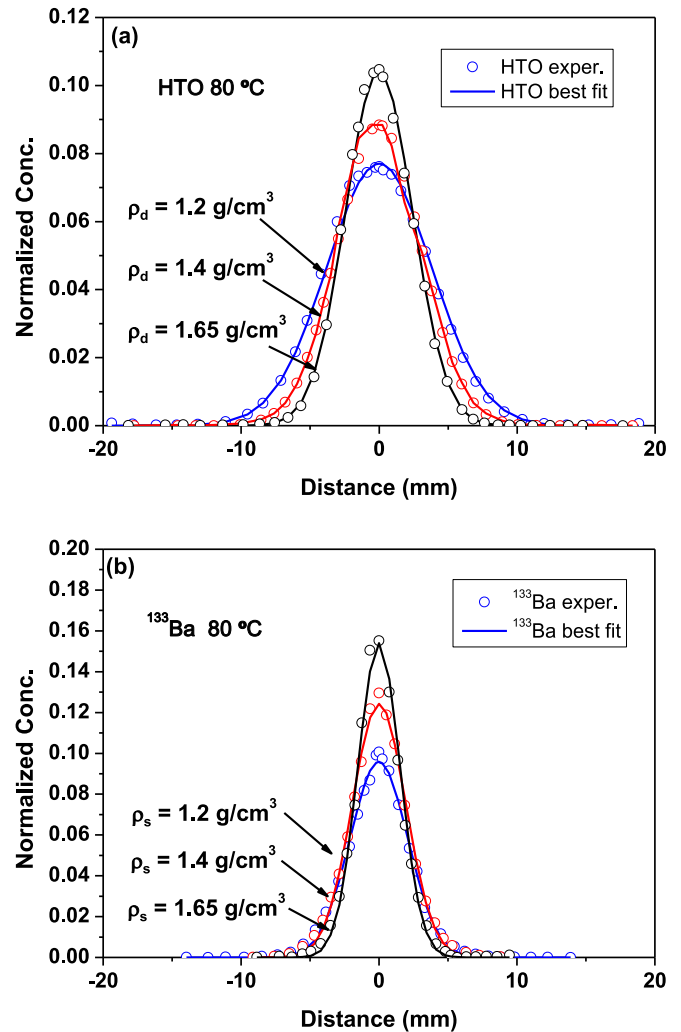
Fig. 2. K_d values obtained as a function of the temperature for Sr (filled symbols) and Ba (open symbols) in deionized water and porewater at 1.4 and 1.65 g cm^{-3}.

Fig. 3. Comparison of diffusion test carried out at different dry density and fixed temperature. a) HTO, 80 °C and diffusion time 2 h; b) ^{133}Ba, 80 °C and diffusion time 20 h. The continuous lines correspond to the best fit of the data obtained using equation (3).

Table 4

Apparent diffusion coefficients, D_a ($m^2 \cdot s^{-1}$), determined as function of the temperature and dry density. Mean values and errors are obtained considering different replicates of the tests under the same experimental conditions.

HTO			
Temperature (°C)	$\rho_d = 1.2$ g cm^{-3}	$\rho_d = 1.4$ g cm^{-3}	$\rho_d = 1.65$ g cm^{-3}
25	$(3.9 \pm 0.1) \cdot 10^{-10}$	$(2.6 \pm 0.1) \cdot 10^{-10}$	$(1.7 \pm 0.2) \cdot 10^{-10}$
40	$(6.1 \pm 0.3) \cdot 10^{-10}$	$(3.9 \pm 0.3) \cdot 10^{-10}$	$(1.8 \pm 0.2) \cdot 10^{-10}$
60	$(8.7 \pm 0.2) \cdot 10^{-10}$	$(5.3 \pm 0.3) \cdot 10^{-10}$	$(2.7 \pm 0.2) \cdot 10^{-10}$
80	$(1.0 \pm 0.3) \cdot 10^{-9}$	$(6.3 \pm 0.2) \cdot 10^{-10}$	$(4.0 \pm 0.4) \cdot 10^{-10}$
^{36}Cl			
Temperature (°C)	$\rho_d = 1.2$ g cm^{-3}	$\rho_d = 1.4$ g cm^{-3}	$\rho_d = 1.65$ g/cm^3
25	$(2.7 \pm 0.2) \cdot 10^{-10}$	$(1.2 \pm 0.1) \cdot 10^{-10}$	$(5.7 \pm 0.2) \cdot 10^{-11}$
40	$(3.3 \pm 0.2) \cdot 10^{-10}$	$(1.6 \pm 0.1) \cdot 10^{-10}$	$(6.2 \pm 0.3) \cdot 10^{-11}$
60	$(5.5 \pm 0.1) \cdot 10^{-10}$	$(2.6 \pm 0.1) \cdot 10^{-10}$	$(9.6 \pm 0.2) \cdot 10^{-11}$
80	$(6.6 \pm 0.3) \cdot 10^{-10}$	$(3.3 \pm 0.1) \cdot 10^{-10}$	$(1.7 \pm 0.2) \cdot 10^{-10}$
^{85}Sr			
Temperature (°C)	$\rho_d = 1.2$ g cm^{-3}	$\rho_d = 1.4$ g cm^{-3}	$\rho_d = 1.65$ g cm^{-3}
25	$(2.2 \pm 0.1) \cdot 10^{-11}$	$(1.7 \pm 0.1) \cdot 10^{-11}$	$(5.0 \pm 0.3) \cdot 10^{-12}$
40	$(3.5 \pm 0.3) \cdot 10^{-11}$	$(2.7 \pm 0.2) \cdot 10^{-11}$	$(7.7 \pm 0.3) \cdot 10^{-12}$
60	$(5.4 \pm 0.4) \cdot 10^{-11}$	$(4.0 \pm 0.3) \cdot 10^{-11}$	$(1.5 \pm 0.2) \cdot 10^{-11}$
80	$(6.7 \pm 0.3) \cdot 10^{-11}$	$(5.4 \pm 0.3) \cdot 10^{-11}$	$(1.8 \pm 0.2) \cdot 10^{-11}$
^{133}Ba			
Temperature (°C)	$\rho_d = 1.2$ g cm^{-3}	$\rho_d = 1.4$ g cm^{-3}	$\rho_d = 1.65$ g cm^{-3}
25	$(1.5 \pm 0.2) \cdot 10^{-11}$	$(9.5 \pm 0.3) \cdot 10^{-12}$	$(3.6 \pm 0.3) \cdot 10^{-12}$
40	$(1.9 \pm 0.2) \cdot 10^{-11}$	$(1.3 \pm 0.3) \cdot 10^{-11}$	$(6.2 \pm 0.3) \cdot 10^{-12}$
60	$(2.8 \pm 0.3) \cdot 10^{-11}$	$(2.2 \pm 0.3) \cdot 10^{-11}$	$(1.1 \pm 0.2) \cdot 10^{-11}$
80	$(3.8 \pm 0.3) \cdot 10^{-11}$	$(2.9 \pm 0.2) \cdot 10^{-11}$	$(1.6 \pm 0.2) \cdot 10^{-11}$

of HTO. Moreover, the distance travelled within the clay increases with lower dry densities for all elements, resulting in smaller D_a values for higher dry densities due to the lower number of water layers in the interlayer and, consequently, a lower volumetric water content (Kozaki et al., 1998).

The values of D_a obtained with the instantaneous planar source method for HTO and ^{36}Cl$^-$ are in good agreement with previous studies conducted on the same material, which analysed the impact of clay density on diffusion at room temperature using traditional through-diffusion techniques (García-Gutiérrez et al., 2004). It is remarkable that the planar source method utilized in this study has an advantage, over classical through-diffusion tests that the results are obtained in significantly shorter timeframes (hours instead of several weeks).

The relation between D_a, temperature and dry density is clearly summarized in Fig. 4. In all cases, the increase of temperature results in an increase of D_a (as an "incremental" effect), while increasing the dry density has the opposite effect (as a "decremental" effect). Under the same conditions of temperature and clay dry density D_a values increases in the following order Ba < Sr < Cl < HTO, with D_a values for Ba almost two orders of magnitude lower than those of HTO. For a determined radionuclide, the lowest D_a always corresponds to the lowest temperature and the highest dry density.

The dependence of D_a on the absolute temperature (K) at different dry densities were analysed using the Arrhenius and the Stokes-Einstein equations (Savoye et al., 2011; Mon et al., 2016).

According to the Arrhenius' Law the dependence of D_a on temperature can be written as:

$$D_a(T) = A_r \cdot \exp\left(-\frac{E_a}{R \cdot T}\right) \qquad (4)$$

where A_r is an empirical constant (Arrhenius parameter or pre-exponential factor), E_a the activation energy of the process (kJ·mol^{-1}), T is the absolute temperature (K) and R the gas constant ($8.314 \cdot 10^{-3}$ kJ/K·mol). E_a represents the minimum amount of energy that is required to
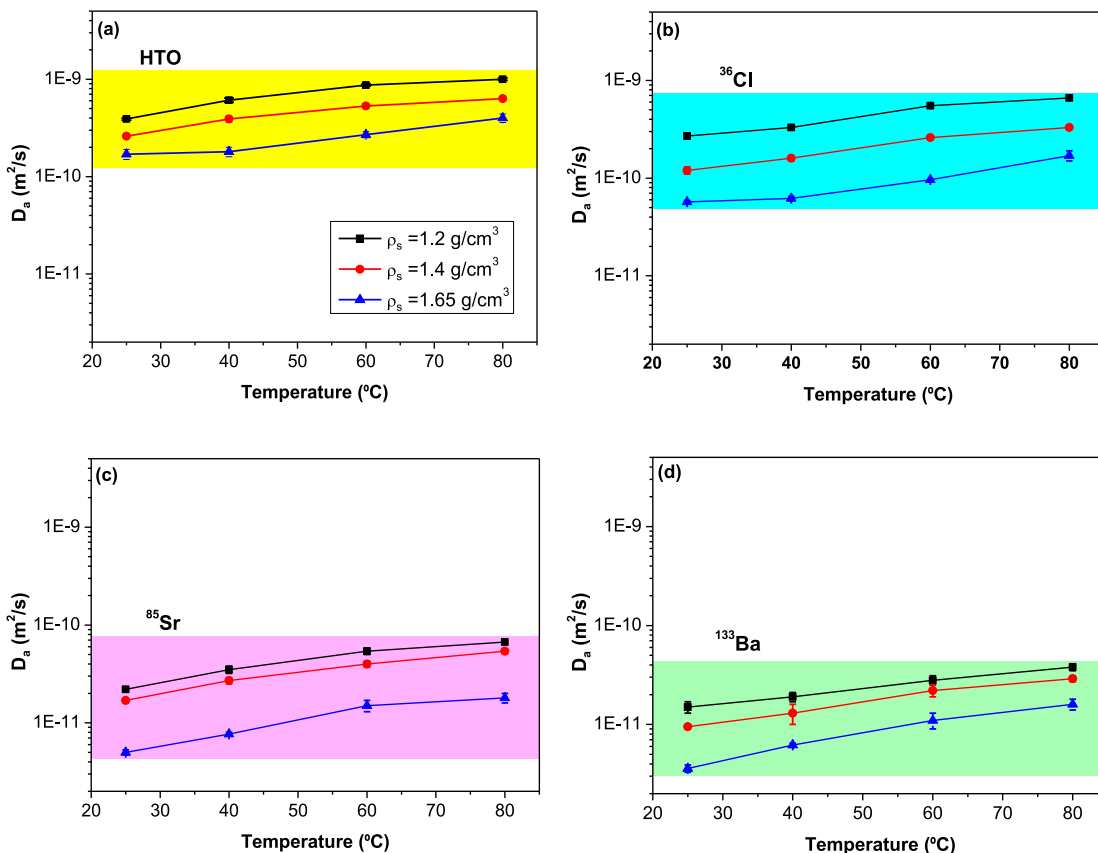

Fig. 4. Summary of the dependence of D_a on temperature and dry density. a) HTO; b) ^{36}Cl; c) ^{85}Sr and d) ^{133}Ba.

activate a process (reaction or physical transport) (González-Sánchez et al., 2008).

This expression can be linearized as:

$$ln\, D_a(T) = ln\, A_r - \frac{E_a}{R}\left(\frac{1}{T}\right) \qquad (5)$$

Expressing D_a values in the logarithmic form *vs.* (1/T), it is possible determining the activation energy from the slope of the linear fit.

The Arrhenius plots for all the RN analysed in this study are shown in Fig. 5, with the best linear fit obtained with equation (5). For all the dry densities and RN type, the Arrhenius' Law describes well the variation of D_a with temperature, observed experimentally for all RNs.

The activation energies calculated with data in Fig. 5, and the correlation coefficients obtained in each case, are summarized in Table 5. The diffusive behaviour as a function of the temperature could be satisfactorily fit by the Arrhenius' law. The calculated activation energies (E_a) of the different radionuclides exhibit distinct behaviours with respect to dry density. The activation energy represents the energy barrier that must be overcome for diffusion to occur: HTO presents the smallest E_a values, which show little variation and no clear pattern as the dry density changes.

Conversely, Cl, Sr and Ba display a noticeable increase in E_a with increasing dry density, which can be related to the fact that charge (Cl) or steric effect (Sr, Ba), leading to lower effective porosity which hinders transport in highly compacted clay. The adsorption of Sr and Ba seems not to be a determining factor for increasing E_a because, in fact, under the conditions of diffusion experiments, sorption is expected to be relatively low ($K_d < 10$ mL g^{-1} for ^{85}Sr $K_d < 90$ mL g^{-1} for ^{133}Ba), being similar for the two porewaters.

Another important relation between diffusion and temperature is given by the Stokes-Einstein equation:

Table 5
Activation energy obtained from the fit of the data with equation (5).

Tracer	ρ_d (g·cm^{-3})	R-Square	E_a (kJ·mol^{-1})
HTO	1.2	0.925	15.0 ± 2.4
	1.4	0.948	13.9 ± 1.9
	1.65	0.908	14.1 ± 2.5
^{36}Cl	1.2	0.957	15.1 ± 1.8
	1.4	0.983	16.7 ± 1.2
	1.65	0.890	17.6 ± 3.5
^{85}Sr	1.2	0.962	17.8 ± 2.0
	1.4	0.982	18.2 ± 1.4
	1.65	0.949	21.3 ± 2.8
^{133}Ba	1.2	0.995	15.0 ± 0.6
	1.4	0.986	18.3 ± 1.2
	1.65	0.988	23.8 ± 1.5

$$D_0 = \frac{k \cdot T}{6\pi \cdot r_s \cdot \eta} \qquad (6)$$

where k is the Bolzmann constant ($1.38 \cdot 10^{-23}$ J K^{-1}) and r_s the hydrodynamics radius of solute (m), η the viscosity of the fluid (Pa·s) and T the absolute temperature (K). This equation indicates that, the diffusion coefficient in free water, D_0, varies linearly with the temperature and inversely with the viscosity η of the medium.

Knowing the diffusion coefficient at a given reference temperature (T_0), according to equation (6), the diffusion coefficient at another temperature T can be calculated by the following formula:

$$D_a(T) = \left(\frac{T}{T_0}\right)\left(\frac{\mu_{T_0}}{\mu_T}\right) \cdot D_a(T_0) \qquad (7)$$

where $D_a(T_0)$ is the apparent diffusion coefficient at the reference temperature T_0, and μ_{T_0} and μ_T are the dynamic viscosities at
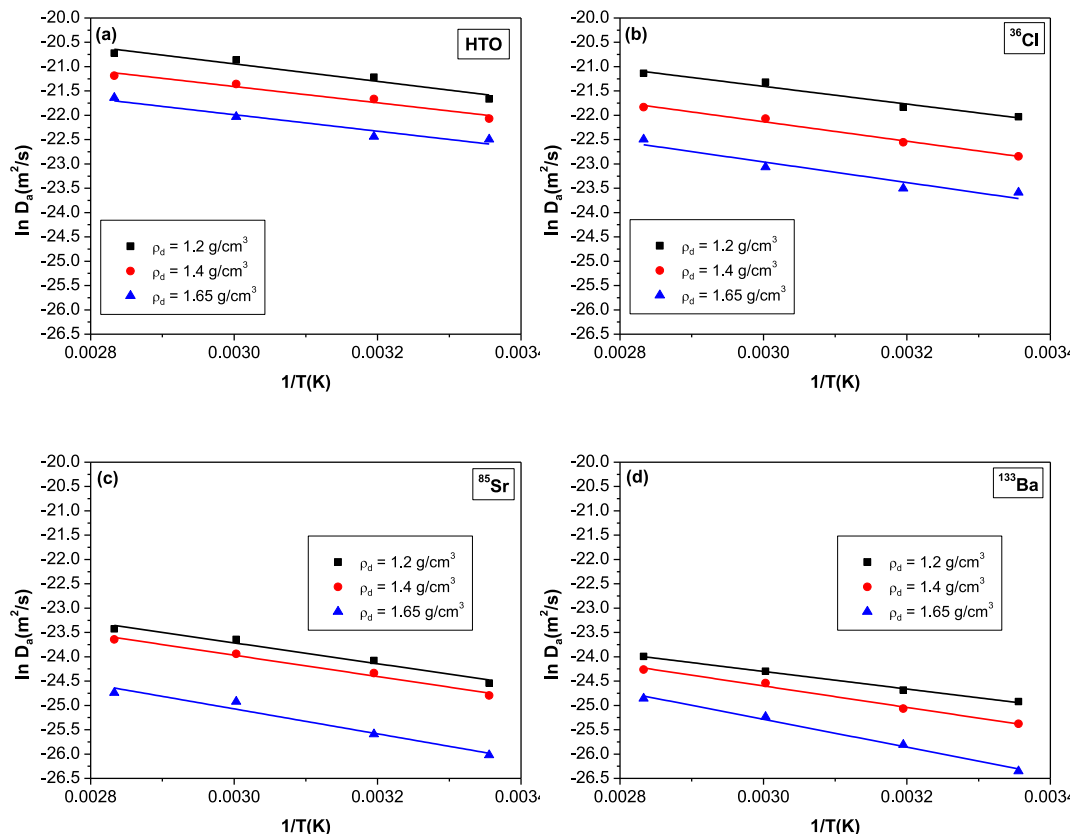

Fig. 5. Arrhenius plots and best linear fit of data. a) HTO, b) ^{36}Cl, c) ^{85}Sr, and d) ^{133}Ba.

temperature T_0 and T, respectively. The temperature of 25 °C (298 K) has been selected as reference temperature. The viscosity of pure water at different temperatures can be estimated using the semi-empirical Vogel-Fulcher-Tammann equation: μ = A·exp (B/(T-C)), where A = 0.02939 mPa s; B = 5007.88 K; and C = 149.3 K (Viswanath & Natarajan, 1989).

Fig. 6 compares the experimental D_a, obtained as a function of the temperature at the three different dry densities (1.2, 1.4 and 1.65 g/cm³; Fig. 6a, b and 6c respectively) and D_a values estimated with equation (7), represented as a star in the graphs.

In general, for the dry densities of 1.2 and 1.4 g·cm⁻³, the calculated D_a values correspond quite well with the experimental with a percentage error lower than 15%, for all the investigated RN. Nevertheless, for the dry density of 1.65 g·cm⁻³, the correspondence between experimental data and calculated values is worst, with errors of up to 35%. Therefore,
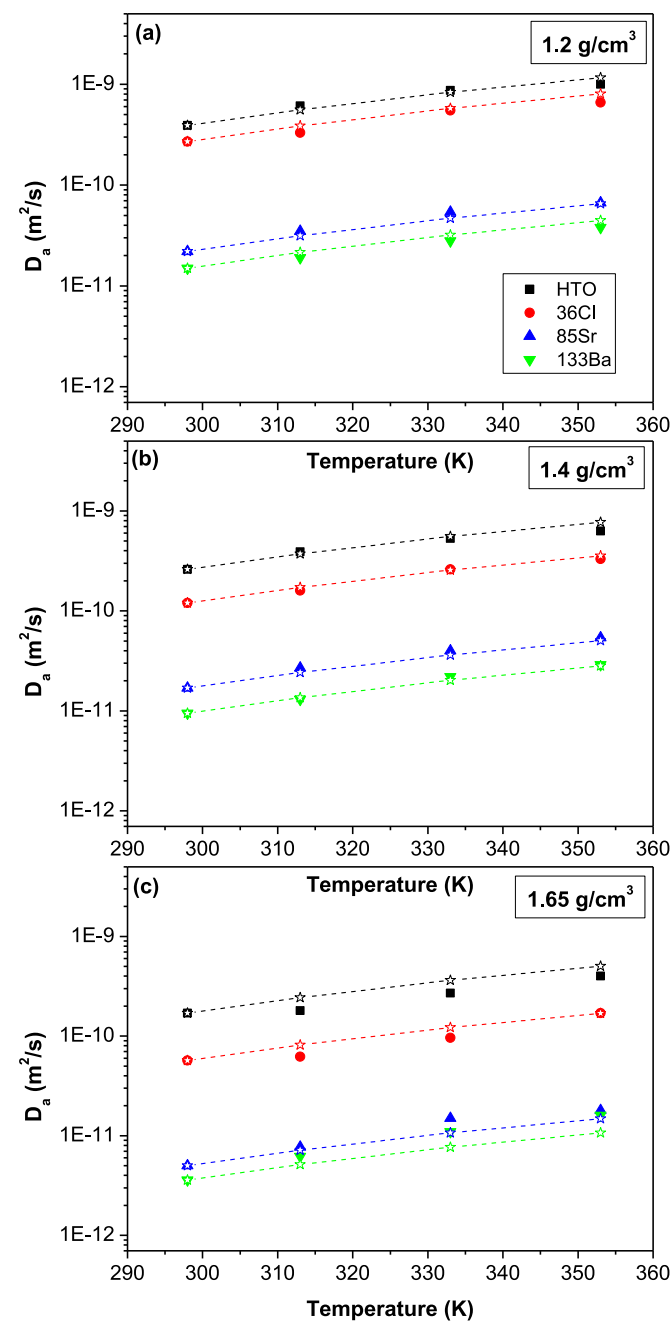
these results indicate that the Stokes-Einstein relationship can be taken as a good approximation to estimate D_a at different temperatures starting from room temperature tests, only when the dry density of the compacted clay is ≤ 1.4 g·cm⁻³. This conclusion agrees with the study of Van Loon et al. (2005), who observed that in consolidated clay, with a density of 2.4 g/cm³, the Stokes-Einstein equation could not be used to describe the temperature dependence experimentally observed for HTO diffusion. Savoye et al. (2011) found that this relation was able to describe the temperature dependence of the diffusion of non sorbing elements (HTO and ³⁶Cl) but failed for sorbing cations (²²Na and ¹³⁷Cs) in consolidated clays at 2.42 g cm⁻³.

The viscosity of water is an important variable parameter in equation (7). Typically, water viscosity decreases with increasing temperature. However, the salinity of clay porewater increases with both the dry density (as shown in Table 1) and the temperature (as shown in Table 2). Higher salinity of most electrolytes typically leads to an increase in water viscosity (Sharqawy et al., 2010), which could explain the observed deviations from the Stokes-Einstein relation. However, the effects of varying ionic strength in complex electrolytes cannot be easily generalized. In addition, the structure of water in compacted clays differs from that of free water; Low (1976) demonstrated that the viscosity of interlayer water is higher than that of bulk water and increases exponentially as the water content decreases.

4. Conclusions

The combined effects of clay density (1.2–1.65 g cm⁻³), temperature (25–80 °C) and porewater chemistry on the apparent diffusion coefficients (D_a) in bentonite have been analysed for radionuclides with different properties (HTO, ³⁶Cl, ⁸⁵Sr, and ¹³³Ba).

D_a values increased with temperature and decreased with dry density, with the highest D_a for each radionuclide observed at the highest temperature and lowest dry density. D_a values increased in the order of Ba < Sr < Cl < HTO under the same dry density and temperature conditions, with D_a values in the range of (0.36–3.80)·10⁻¹¹ m s⁻² for Ba, (0.5–6.7)·10⁻¹¹ m s⁻² for Sr, (0.57 − 6.60)·10⁻¹⁰ m s⁻² for Cl, and (0.17 − 1.00)·10⁻⁹ m s⁻² for HTO.

The activation energy (E_a) of the diffusion process was successfully determined by the application of the Arrhenius' law, which indicated the mayor role of the clay density in hindering radionuclide diffusion. The Stokes-Einstein approximation also reproduced quite well the temperature dependence of D_a for dry densities ≤1.4 gcm⁻³, but the fit was worst for highly compacted clays. A more precise determination of porewater viscosity at different dry densities and temperatures could improve the agreement.

The clay density directly influences water content, thereby affecting the properties of clay pore water and temperature can also impact on the dissolution of soluble salts (water salinity) and viscosity. Thus, the control of porewater chemistry in diffusion test is an issue to be explicitly considered.

CRediT authorship contribution statement

Miguel García-Gutiérrez: Writing – review & editing, Writing – original draft, Methodology, Investigation, Formal analysis, Data curation, Conceptualization. **Manuel Mingarro:** Investigation, Formal analysis, Data curation. **Tiziana Missana:** Writing – review & editing, Writing – original draft, Investigation, Funding acquisition, Formal analysis.

Declaration of competing interest

The authors declare that they have no known competing financial interests or personal relationships that could have appeared to influence the work reported in this paper.

Fig. 6. Measured D_a values and calculated values (-☆-) using the Stokes-Einstein equation. Dry density: a) 1.2 g cm⁻³; b) 1.4 g cm⁻³ and c) 1.65 g cm⁻³.

Data availability

Data will be made available on request.

Acknowledgments

This work has been partially supported by the European Union's Horizon 2020 research and innovation programme under Grant Agreement n° 847593 (EURAD) and by the Spanish Ministry of Innovation and Science (PID2022-138402NB-C22, ACOMER project).

References

Aldaba, D., García-Gutiérrez, M., Rigol, A., Vidal, M., 2010. Comparison of laboratory methodologies for evaluating radiostrontium diffusion in soils: planar-source versus half-cell methods. Sci. Total Environ. 408, 5966–5971.

Andra, 2001. Dossier 2001 Argile. Progress report on the feasibility studies and research into deep geological disposal of high level, long-lived waste. Synthesis report. Andra Report Series, p. 92.

Andra, 2005. Andra research on the geological disposal of high level long-lived radioactive waste. Report Series, Dossier 2005 Andra, Paris, France, p. 15.

Bestel, M., Glaus, M.A., Frick, S., Gimmi, T., Juranyi, F., Van Loon, L.R., Diamond, L.W., 2018. Combined tracer through-diffusion of HTO and 22Na through Na-montmorillonite with diferent bulk dry densities. Appl. Geochem. 93, 158–166.

Crank, J., 1975. The Mathematics of Diffusion, second ed. Clarendon Press, Oxford.

Enresa, 1999. Evaluación del Comportamiento y de la Seguridad de un Almacenamiento Profundo en Arcilla. Publicación Técnica 03/99. ENRESA, Madrid, España.

Fernández, A.M., Rivas, P., 2004. Pore water chemistry of saturated FEBEX bentonite compacted at different densities. In: Advances in Understanding Engineered Clay Barriers. A.A. Balkema Publishers.

García-Gutiérrez, M., Cormenzana, J.L., Missana, T., Alonso, U., Mingarro, M., 2011. Diffusion of strongly sorbing cations (^{60}Co and ^{152}Eu) in compacted FEBEX bentonite. Phys. Chem. Earth 36, 1708–1713.

García-Gutiérrez, M., Cormenzana, J.L., Missana, T., Mingarro, 2004. Diffusion coefficients and accessible porosity for HTO and ^{36}Cl in compacted FEBEX bentonite. Appl. Clay Sci. 26, 65–73.

García-Gutiérrez, M., Cormenzana, J.L., Missana, T., Mingarro, M., Molinero, J., 2006. Overview of laboratory methods employed for obtaining diffusion coefficients in FEBEX compacted bentonite. J. Iber. Geol. 32 (1), 37–53.

González-Sánchez, F., Van Loon, L.R., Gimmi, Th, Jakob, A., Glaus, M.A., Diamond, L.W., 2008. Self-diffusion of water and its dependence on temperature and ionic strength in highly compacted montmorillonite, illite and kaolinite. Appl. Geochem. 23, 3840–3851.

Huertas, F., Fariña, P., Farias, J., García-Siñeriz, J.L., Villar, M.V., Fernández, A.M., Martín, P.L., Elorza, F.J., Gens, A., Sánchez, M., Lloret, A., Samper, J., Martínez, M. A., 2006. Full-scale Engineered Barriers Experiment. Updated Final Report 1994-2004. Enresa PT 05/2006.

Huertas, F., Fuentes-Cantillana, J.L., Jullien, F., Rivas, P., Linares, J., Fariña, P., Ghoreychi, M., Jockwer, N., Kickmaier, W., Martínez, M.A., Samper, J., Alonso, E., Elorza, F.J., 2000. Full-scale engineered barriers experiment for a deep geological repository for high-level radioactive waste in crystalline host rock (FEBEX project). Nuclear Science and Technology. EUR 19147 EN.

Idemitsu, K., Kozaki, H., Yuhara, M., Arima, T., Inagaki, Y., 2016. Diffusion behaviour of selenite in purified bentonite. Prog. Nucl. Energy 92, 279–285.

JNC, 1999. H12 project to establish technical basis for HLW disposal in Japan. Project Overview Report. JNC Technical Report, TN 1400, 99–9010.

Joseph, C., Mibus, J., Trepte, P., Müller, Ch, Brendler, V., park, D.M., Jiao, Y., Kersting, A., Zavarin, M., 2017. Long-term diffusion of U(VI) in bentonite: dependence on density. Sci. Total Environ. 575, 207–218.

Joseph, C., Van Loon, L.R., Jakob, A., Steudtner, R., Schmeide, K., Sachs, S., Bernhard, G., 2013. Diffusion of U(VI) in Opalinus clay: influence of temperature and humic acid. Geochem. Cosmochim. Acta 109, 74–89.

Kasar, S., Kumar, S., Bajpai, R.K., Tomar, B.S., 2016. Diffusion of Na(I), ca(I), Sr(II) and Eu(III) in smectite rich natural clay. J. Environ. Radioact. 151, 218–223.

Kozaki, T., Fujishima, A., Sato, S., 1998. Self-diffusion of sodium ions in compacted sodium montmorillonite. Nucl. Technol. 121, 63–69.

Kozaki, T., Inada, K., Sato, S., Ohashi, H., 2001. Diffusion mechanism of chloride ions in sodium montmorillonite. J. Contam. Hydrol. 47, 159–170.

Low, P.F., 1976. Viscosity of interlayer water in montmorillonite. Soil Sci. Soc. Am. J. 40, 500–505.

Medved, I., Černý, R., 2019. Modeling of radionuclide transport in porous media: a review of recent studies. J. Nucl. Mater. 526, 151763.

Mon, E.E., Hamamoto, S., Kawamoto, K., Komatsu, T., 2016. Temperature effects on solute diffusion and adsorption in differently compacted kaolin clay. Environ. Earth Sci. 75, 562.

Nagra, 2002. Project Opalinus Clay: Safety Report–Demonstration of Disposal Feasibility for Spent Fuel, Vitrified High-Level Waste and Long-Lived Intermediate-Level Waste. Nagra Technical Report NTB-02-05, Wettingen, Switzerland.

NEA, 2003. Engineered Barrier Systems and the Safety of Deep Geological Repositories, State-Of-The-Art Report. OECD-NEA. Paris.

Pope, R.N., 2017. Influence of Temperature on Diffusion and Sorption of 237Np(V) through Bentonite Engineered Barriers. Clemson University, USA. Thesis presented at.

Posiva, 2012. Safety Case for the Disposal of Spent Nuclear Fuel at Olkiluoto - Synthesis 2012 Posiva Reports, vols. 2012–12. Olkiluoto, Finland, Posiva, p. 324.

Rowe, R.K., Mukunoki, T., Sangam, H., 2005. BTEX diffusion and sorption for a Geosynthetic Clay Liner at two temperatures. J. of Geotechnical and Environmental Engineered 1211–1221.

Savoye, S., Goutelard, F., Beaucaire, C., Charles, Y., Fayette, A., Herbette, M., Larabi, Y., Coelho, D., 2011. Effect of temperature on the containment properties of argillaceous rocks: the case study of Callovo-Oxfordian claystones. J. Contam. Hydrol. 125, 102–112.

Sellin, P., Leupin, O., 2014. The use of clay as an engineered barrier in radioactive waste management – a review. Clay Clay Miner. 61, 477–498.

Sharqawy, M.H., Lienhard, J.H., Zubair, S.M., 2010. The thermophysical properties of seawater: a review of existing correlations and data.". Desalination Water Treat. 16 (1–3), 354–380.

SKB, 2011. Long-term Safety for the Final Repository for Spent Nuclear Fuel at Forsmark. Main Report of the SR-Site Project. Volume II. SKB Technical Reports, TR-11-01, SKB, Stockholm, Sweden, p. 278.

Suzuki, S., Sato, H., Ishidera, T., Fujii, N., 2004. Study on anisotropy of effective diffusion coefficient and activation energy for deuterated water in compacted sodium bentonite. J. Contam. Hydrol. 68, 23–37.

Van Loon, L.R., Müller, W., Iijima, K., 2005. Activation energies of the selfdiffusion of HTO, 22Na and 36Cl in a highly compacted argillaceous rock (Opalinus Clay). Appl. Geochem. 20, 961–972.

Van Loon, L.R., Soler, J.M., Müller, W., Bradbury, M.H., 2004. Anisotropic diffusion in layered argillaceous rocks: a case study with Opalinus Clay. Environ. Sci. Technol. 38 (21), 5721–5728.

Villar, M.V., Gómez-Espina, R., Lloret, A., 2010. Experimental investigation into temperature effect on hydro-mechanical behaviour of bentonite. J. Rock Mech. Geotech. Eng. 2 (1), 71–78.

Viswanath, D.S., Natarajan, G., 1989. Data Book on the Viscosity of Liquids. Hemisphere Publishing Corporation. ISBN 0-89116-778-1.

Xiang, Y., AI, T., Mazurek, M., 2016. Effect of confining pressure on diffusion coefficients in clay-rich, low-permeability sedimentary rocks. J. Contam. Hydrol. 195, 1–10.

Yang, W., Zheng, Y., Zaoui, A., 2015. Swelling and diffusion of Na-vermiculite at different hydrated states. Solid State Ionics 282, 13–17.

Zheng, Y., Zaoui, A., 2013. Temperature effects on the diffusion of water and monovalent counterions in the hydrated montmorillonite. Phys. Stat. Mech. Appl. 392, 5994–6001.